

INTEGRAL FIELD SPECTROSCOPY OF FAINT HALOS OF PLANETARY NEBULAE

A. MONREAL-IBERO,¹ M. M. ROTH,^{1,2} D. SCHÖNBERNER,¹ M. STEFFEN,¹ AND P. BÖHM¹

Received 2005 March 29; accepted 2005 June 13; published 2005 July 11

ABSTRACT

We present the first integral field spectroscopy observations of the two planetary nebulae NGC 3242 and NGC 4361 with the VIMOS instrument attached to VLT-UT3. By co-adding a large number of spaxels, we reach an emission-line detection limit of 5×10^{-18} ergs cm⁻² s⁻¹ arcsec⁻². In the case of NGC 3242, we succeed in determining some properties of the halo. The radial surface brightness profile in [O III] implies increasing mass loss before the formation of the planetary nebula. Traces of the mysterious “rings” are clearly visible. We find for the first time an apparent temperature gradient across a halo: from about 16,000 K close to the shell/halo transition to 20,000 K at the halo’s outer edge. No line emission is seen in the suspected halo region of NGC 4361 down to the sensitivity limit.

Subject heading: planetary nebulae: individual (NGC 3242, NGC 4361)

1. INTRODUCTION

Next to supernova explosions, stellar winds on the asymptotic giant branch (AGB) make significant contributions to the recycling of chemically enriched material to the interstellar medium. The physics of AGB mass loss is therefore a key ingredient for our understanding of the evolution of galaxies, as far as the recycling of matter, processed by different stellar populations, is concerned. Despite considerable progress in our theoretical understanding of stellar evolution and mass loss during the last AGB phase, observational details of this critical period have remained obscure. Halos of planetary nebulae (PNe) are fossil records of the mass-loss history at the tip of the AGB, which, in principle, can be investigated with the plasma diagnostic tools for gaseous nebulae. However, spectroscopy of these low surface brightness regions is extremely difficult to perform with conventional slit spectrographs.

Encouraged by successful experiments with the Potsdam Multi-Aperture Spectrophotometer (PMAS; Roth et al. 2004, 2005), we have employed the technique of integral field spectroscopy (IFS) to obtain unprecedented sensitivity for the measurement of PN emission-line intensities, by co-adding many spatial elements (spaxels) over the field of view (FOV) of an integral field unit (IFU). We have used the unique light-collecting properties of the VISIBLE Multi-Object Spectrograph (VIMOS) IFU at the Very Large Telescope (VLT) for a plasma diagnostic analysis of selected targets from the catalog of PN halos of Corradi et al. (2003) with the goal of measuring the n_e , T_e , and chemical composition in order to test the most recent theoretical predictions.

Here we present first results from the spatially resolved spectrophotometry on the outskirts of NGC 4361, which is a low-metallicity Galactic halo object, and of the disk PN NGC 3242. Both objects are well-developed PNe with central stars of very similar effective temperatures, viz., of 75,000 K for NGC 3242 and 82,000 K for NGC 4361 (Méndez et al. 1992). NGC 3242 has a well-defined halo at the percent level of the peak surface brightness (Corradi et al. 2003), where recently mysterious “rings” have been detected (Corradi et al. 2004). To date, no halo has been reported for NGC 4361. Also, due to its low metal

content, the electron temperature of NGC 4361 ($\approx 19,000$ K) is unusually large (Torres-Peimbert et al. 1990).

2. OBSERVATIONS

We performed VLT observations with the unit telescope “Melipal” (UT3) on 2004 April 17 and 18 using the VIMOS-IFU. The instrument was set up in the LR_blue mode with a spaxel scale of 0'67, a FOV of 54" \times 54", a nominal wavelength range of 3700–6700 Å, 5.3 Å pixel⁻¹ reciprocal dispersion, and a spectral resolution of $R \approx 180$. Both nights were photometric, with a seeing of $\approx 1''.3$ and $\approx 1''.0$ FWHM, respectively. We observed each object with a series of snapshot exposures centered on the central star, in order to obtain a reference on the bright part of the nebula, and a series of deep exposures in one or two halo fields as the major objective of this run: 3 \times 100 s centered on NGC 3242, 3 \times 900 s offset by 55" and 63" to the west (halo fields), 2 \times 2 mosaic centered on NGC 4361 with 300 s each, and 2 \times 900 s adjacent to this mosaic to the west (see Figs. 1 and 2). Internal continuum and arc lamp flat-field exposures as well as spectrophotometric standard-star exposures were taken throughout the night.

3. DATA REDUCTION

The data reduction was performed with a modified subset of routines from the PMAS P3d pipeline (Becker 2002; Roth et al. 2005). An input list of data and calibration files was processed by an IDL script such that each of the four VIMOS channels was treated separately, dissecting each CCD frame into four subfields that correspond to a bank of spectra from the same pseudoslit. Thus, a total of 16 subfields were piped into the P3d routines, which then operated like it does with ordinary PMAS frames.

The data reduction proceeded as follows: First, the bias level was subtracted, and cosmic-ray hits were removed. Second, a trace mask was generated from an internal continuum calibration lamp exposure, identifying the location of each spectrum on the CCD along the direction of dispersion. In order to make this procedure robust, it was necessary to truncate the spectra on each side and discard regions with contamination from adjacent spectra of a neighboring bank. Since VIMOS calibration spectra are taken only when the telescope is pointing to the zenith, and because of the presence of significant flexure, the trace mask had to be shifted in x and y to match the location of the actual

¹ Astrophysikalisches Institut Potsdam, An der Sternwarte 16, D-14482 Potsdam, Germany; amonreal@aip.de.

² Visiting Astronomer at the European Southern Observatory, Chile (ESO proposal 073.D-0576).

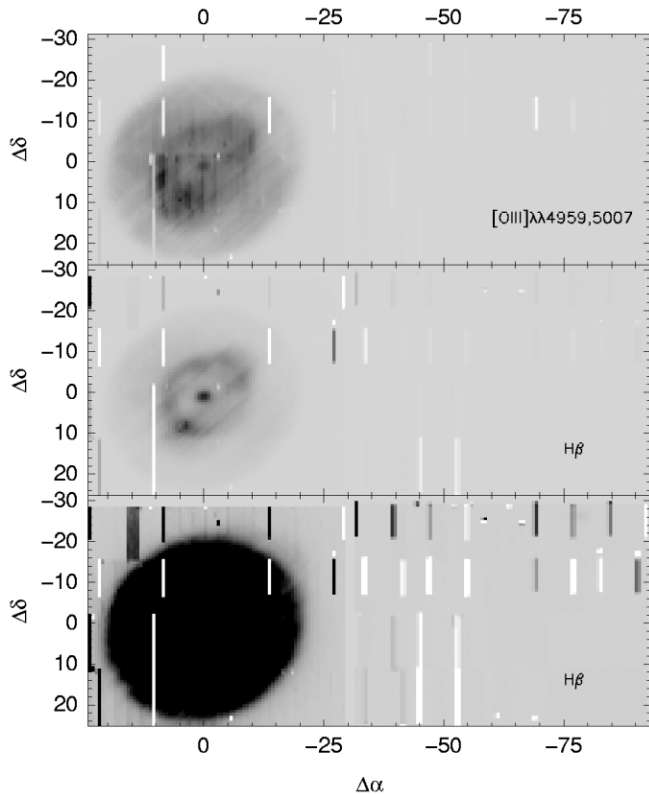


FIG. 1.—Maps of NGC 3242 in [O III] $\lambda\lambda 4959, 5007$ (top), H β low contrast (middle), and H β high contrast (bottom). The mosaic was constructed from shallow pointings, centered on the PN, and two overlapping deep pointings to the west. Artifacts are discussed in text. North is up, and east is left.

science exposure. The offset for this task was obtained from a cross-correlation between the calibration lamp and the science exposure. Third, the 6400 spectra were extracted using a simple swath extraction technique (no profile fitting). After this, the data had changed from a CCD-based format to the so-called row-stacked-spectra (RSS) format, which is a two-dimensional image where each row represents a spectrum. As the fourth step, the RSS frame was wavelength-calibrated with an arc exposure, which turned out to be a critical step since spectral line artefacts (zero and higher order contamination) sometimes confused the P3d line search algorithm. The last step consisted in a correction of the spectrum-to-spectrum sensitivity variation, which was performed by dividing by an extracted and normalized continuum lamp flat-field exposure.

Flux calibration was performed from a series of standard-star exposures that were taken in different quadrants of the IFU in order to obtain an idea of the achievable accuracy. There is considerable scatter, indicating that the flux calibration is not uniform over the face of the IFU. Second, an inspection of the standard deviation as a function of wavelength shows that only within a window of [4200, 6100 Å] is the variation reasonably behaved ($\approx 15\%$ rms). The region of the spectra beyond 6100 Å presents an artifact probably due to contamination of other orders. In addition, wavelength calibration in this range was not accurate enough, and some spectra lacked a red continuum for H α , thus preventing us from using this line in the analysis.

4. RESULTS AND DISCUSSION

4.1. Maps, IFU Defects, PN Morphologies

Figures 1 and 2 show maps of NGC 3242 and NGC 4361 in the emission lines of [O III] $\lambda\lambda 4959, 5007$ and H β , respec-

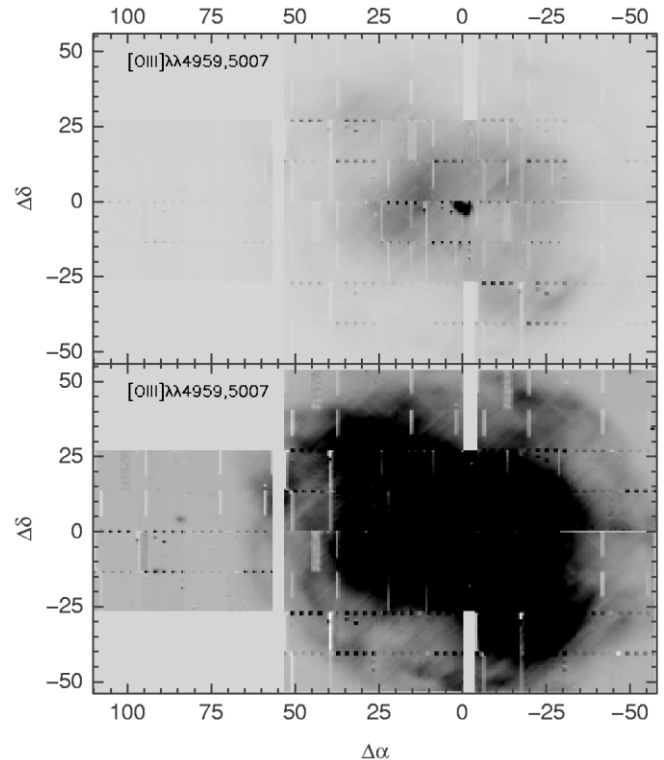


FIG. 2.—Maps of NGC 4361 in [O III] $\lambda\lambda 4959, 5007$. The mosaic constructed from five shallow pointings, centered on the PN, and one deep pointing offset to the east. Low contrast (top), high contrast (bottom). North is up, and east is left.

tively. Various IFU defects are scattered over the FOV as distinct rectangles, which needed to be discarded from the subsequent analysis. The limited accuracy of the calibration of the spaxel-to-spaxel response variation is visible in some vertical or diagonal intensity enhancements, e.g., in the [O III] $\lambda\lambda 4959, 5007$ and H β frames of NGC 3242.

Despite these cosmetic limitations, the fundamental morphological appearance as described in Corradi et al. (2003) is clearly visible as far as the brighter parts of the nebulae are concerned: central star, central cavity with enhanced rim, and shell. This gross morphology can be fully explained by the combined action of the thermal pressure due to the heating of the nebular gas by photoionization and of the dynamical pressure exerted by the fast stellar wind (see Perinotto et al. 2004). As can be seen from the Figures 1 and 2, the surface brightness distribution of NGC 4361 appears to be much smoother, with no clear distinction between rim and shell. This difference in morphology may well be caused by the low metallicity, since it is known that stellar winds become less vigorous for metal-poor stars (see Vink et al. 2001). A faint halo is not directly visible in any of the maps at the chosen contrast level.

4.2. Emission-Line Intensities, Radial Profiles

Figure 3 shows observed and continuum-subtracted radial profiles in [O III] $\lambda\lambda 4959, 5007$ along right ascension and declination axes. The faint nebular continuum and emission lines make an appreciable background contribution, which is roughly a factor of 50 below the [O III] lines' intensity but which becomes negligible as the former approaches the level of the night-sky continuum background. For NGC 3242, this happens beyond a radial distance of $\approx 40''$ from the central star, from where we have chosen an average as an estimate of the

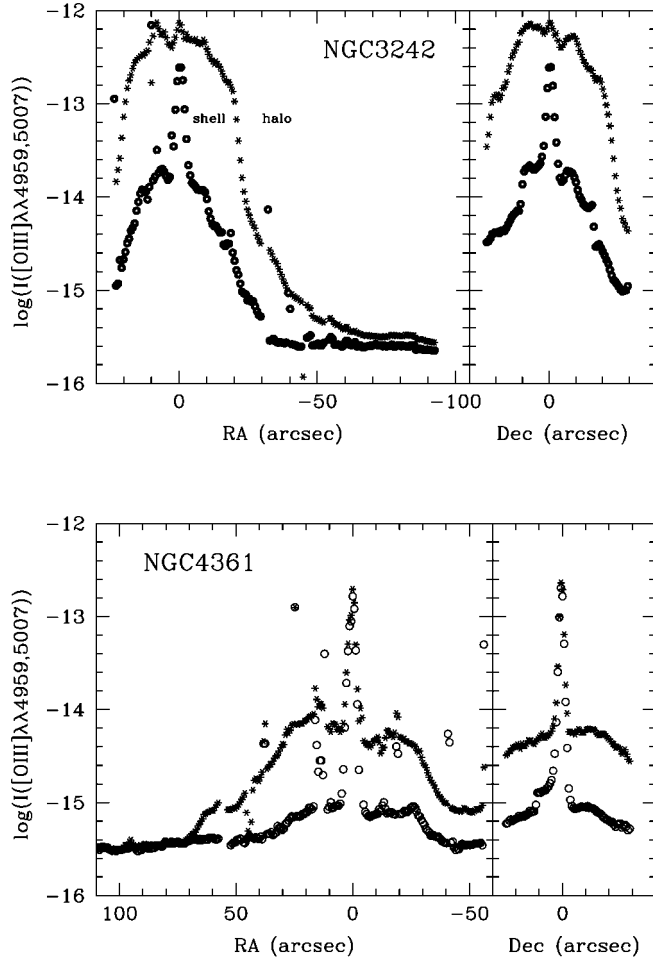


FIG. 3.—Radial intensity profiles in [O III] + background (*asterisks*) and background (*circles*) for NGC 3242 (*top*) and NGC 4361 (*bottom*), from central cuts one spaxel wide and along right ascension and declination. The [O III] $\lambda\lambda 4959, 5007$ emission-line intensity is integrated over the interval 4900–5068 Å; the background is determined from the interval 5100–5150 Å and corrected for the different bandwidth. The intensity scale is in units of $\text{ergs cm}^{-2} \text{s}^{-1} \text{arcsec}^{-2}$.

true sky background at the wavelength of the [O III] lines (NGC 4361: also beyond $\approx 40''$). Using this procedure, we measure the averaged halo [O III] $\lambda\lambda 4959, 5007$ intensity, corrected for sky, as $4.1 \times 10^{-16} \text{ ergs cm}^{-2} \text{s}^{-1} \text{arcsec}^{-2}$, which is a factor of ≈ 2000 below the intensity of the rim. For NGC 4361, having a more than 2 orders of magnitude fainter surface brightness than NGC 3242, no halo emission is seen in Figure 3.

In order to increase the sensitivity for the outer halo regions, we co-added many spaxels over extended regions beyond the shell to obtain an estimate of the average emission line intensity of the halo. Figure 4 illustrates the results. For NGC 3242, the average spectrum clearly confirms the presence of an emission-line halo. Besides the detection of $\text{H}\beta$, which is blended with a sky background feature, there is also the line blend of $\text{H}\gamma$ and [O III] $\lambda 4363$, the latter being important for measuring the electron temperature. We have measured mean intensities for $\text{H}\gamma$, [O III] $\lambda 4363$, $\text{H}\beta$, and [O III] $\lambda\lambda 4959, 5007$ of (8.9, 9.9, 19.8, 411.9) and (51.4, 66.8, 114.7, 4426.4) $\times 10^{-18} \text{ ergs cm}^{-2} \text{s}^{-1} \text{arcsec}^{-2}$ for the outer and inner region of the halo, respectively. Obviously, the accuracy of this result would benefit significantly from higher spectral resolution, e.g., the VIMOS-IFU HR modes, offering a 10-fold higher resolving power than our current data, at the expense of a 4 times smaller FOV.

In the case of NGC 4361, however, there is no detection of

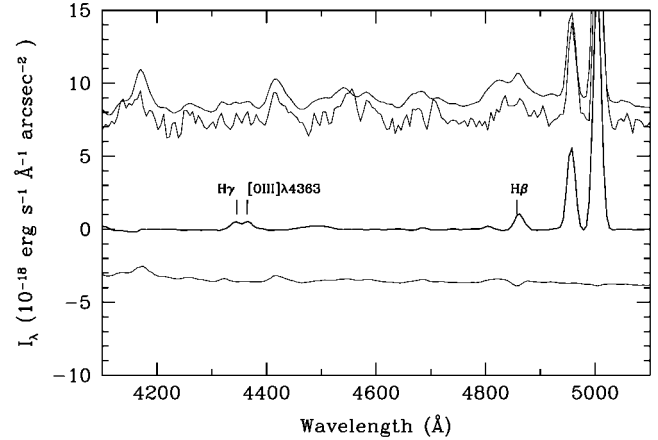


FIG. 4.—Mean halo spectra of NGC 3242 and NGC 4361, averaged from a total of 4547 and 4312 spectra, respectively, and plotted in units of $10^{-18} \text{ ergs cm}^{-2} \text{s}^{-1} \text{Å}^{-1} \text{arcsec}^{-2}$. From top to bottom: NGC 3242 co-added (shifted by $+1 \times 10^{-18} \text{ ergs cm}^{-2} \text{s}^{-1} \text{Å}^{-1} \text{arcsec}^{-2}$), NGC 3242 single spaxel, NGC 3242 co-added + sky-subtracted, NGC 4361 co-added + sky-subtracted spectrum (shifted by $-5 \times 10^{-18} \text{ ergs cm}^{-2} \text{s}^{-1} \text{Å}^{-1} \text{arcsec}^{-2}$).

halo line emission. We derived the detection limit by simulating emission lines with different intensities, which were superposed on the co-added NGC 4361 spectrum, and by attempting to recover these lines with Gaussian fits. Our detection limit estimate in the halo of NGC 4361 is $5 \times 10^{-18} \text{ ergs cm}^{-2} \text{s}^{-1} \text{arcsec}^{-2}$. This value is not quite 2 orders of magnitude below the rim surface brightness; i.e., it is not sufficient for the typical intensity contrast of $\approx 10^3$ (Corradi et al. 2003). Also for this object, suppressing the sky background with higher spectral resolution would significantly lower the detection limit, most probably down to the expected halo surface brightness on the order of $1 \times 10^{-18} \text{ ergs cm}^{-2} \text{s}^{-1} \text{arcsec}^{-2}$.

4.3. The Halo of NGC 3242

The background-subtracted intensity profile in [O III] $\lambda\lambda 4959, 5007$ for the halo of NGC 3242 is shown in Figure 5. We attribute small intensity “bumps” to the existence of the so-called halo rings found recently in a number of PNe (Balick et al. 2001; Corradi et al. 2004). The agreement with the radial positions

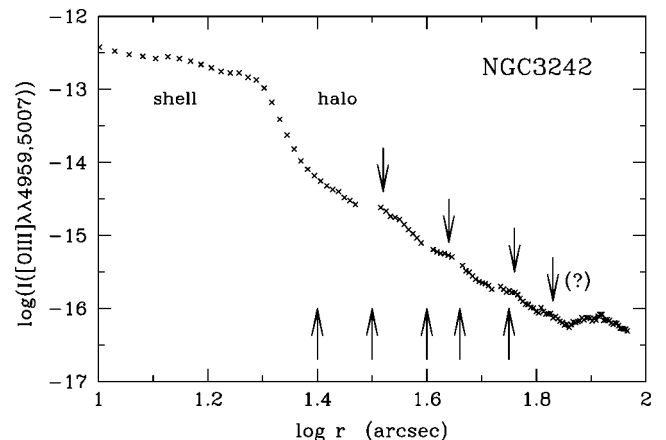


FIG. 5.—Radial background-subtracted [O III] $\lambda\lambda 4959, 5007$ intensity profile for NGC 3242, one spaxel wide, along right ascension, in units of $\text{ergs cm}^{-2} \text{s}^{-1} \text{arcsec}^{-2}$. The shell-halo transition is at a distance of $\approx 22''$ from the center. The vertical arrows indicate the position of the rings from our cut (*downward*) and from R. L. M. Corradi et al. (2004, private communication) (*upward*). The gaps are due to the defects of the IFU.

given by Corradi et al. is good, except in a few cases. We have no indication of a “ring” at 25”, and instead of the two rings at 40” and 46” we found only one located at a radial distance of 43”. Our marginal detection at ≈ 67 ” corresponds to an arc visible in Figure 1 of Corradi et al. at a position angle of $\sim 0^\circ$ – 40° , but it is not annotated as a ring by the authors.

The halo of NGC 3242 is obviously limb-brightened, as the wide bump around 80” indicates. These halos are very common and are explained by hydrodynamical effects when a strong AGB wind interacts with slower, less dense matter expelled earlier during the aftermath of a helium shell flash (Schönberner & Steffen 2002). Matter piles up into a denser shell that, once ionized, is responsible for the bright limb of the halo.

The overall slope of the halo brightness, however, is constant and can well be approximated by a power-law representation, $I \propto r^{-\beta}$, with $\beta = 4.5$. With the reasonable assumption that in the halo, all the oxygen is doubly ionized, one can deduce the radial density profile of the halo as a power-law profile $n(r) \propto r^{-2.8}$. Such a rather strong density decline with distance from the star is consistent with the rather large shell expansion velocity of 36 km s^{-1} and hints at a strongly increasing mass loss toward the end of the AGB evolution (cf. Schönberner et al. 2005, Fig. 13 therein).

We determined the electron temperature, T_e , from the [O III] lines in the vicinity of the main body of the PN and at the outer edge of the halo, employing the low-density limit, using a value for the extinction of $c = 0.15$ (Balick et al. 1993) and the extinction curve of Fluks et al. (1994). We found an apparent temperature gradient across the halo: close to the PN shell (R.A. ≥ -25 ”, with 766 spaxels), we have $T_e = 15,700 \text{ K}$, and at the halo’s edge (R.A. ≤ -60 ”, with 4547 spaxels), $T_e = 20,300 \text{ K}$. For comparison, we also determined the electron temperatures of the rim (i.e., the bright part of the PN) and the shell and found, as averages over 5×5 spaxels, $T_e = 12,000$ and $T_e = 11,000 \text{ K}$, respectively, in good agreement with the determinations of Balick et al. (1993). Our error estimates are $+2000$, -1200 K for the halo and $+600$, -500 K for the PN.

The existence of hot halos has already been reported in the past for NGC 6543, NGC 6826, and NGC 7662 (Middlemass et al. 1989, 1991), based on long-slit observations. The (mean)

halo temperatures range from 13,000 to 17,500 K, but temperature gradients have not been established. High temperatures in the halo can easily be set up by the rapid passage of an ionization front once the main PN becomes optically thin for ionizing photons (Marten 1993). Due to the low densities, the halo matter is far from being in thermal equilibrium, and a positive radial temperature gradient will develop because the cooling rate depends on density squared. Judging from the existence of hot halos around PNe with quite different evolutionary stages, the cooling times seem to be comparable to the nebular lifetime, an important constraint for hydrodynamic models.

5. SUMMARY AND CONCLUSIONS

IFS has been shown to be capable of performing spatially resolved spectrophotometry down to sky-limited intensity levels. We have been able to find halo emission lines down to a detection limit of $5 \times 10^{-18} \text{ ergs cm}^{-2} \text{ s}^{-1} \text{ arcsec}^{-2}$, with positive detections of [O III] $\lambda\lambda 5007, 4959$, [O III] $\lambda 4363$, and H β in the halo of NGC 3242. We confirmed the existence of the mysterious rings and found, for the first time, an apparent electron temperature gradient across the halo that, if confirmed, poses a challenge for evolutionary models of planetary nebulae. Halos are obviously not in thermal equilibrium, making a plasma analysis based on steady state photoionization models highly questionable. From the steep radial intensity profile of the halo, it follows that the mass-loss rate must have increased until the very end of the AGB evolution. No emission line is seen in the putative halo region of NGC 4361 down to the sensitivity limit. Owing to the low surface brightness of this PN, the expected halo is too faint to be detected with the present low-resolution observing mode.

The authors would like to thank the referee, R. Corradi, for helpful comments on the manuscript. A.M.-I. acknowledges support from the Euro3D Research Training Network, funded by the EC (HPRN-CT-2002-00305). Part of this work was supported by the ULTROS project, funded by the German Verbundforschung (05AE2BAA/4).

REFERENCES

- Balick, B., Rugers, M., Terzian, Y., & Chengalur, J. N. 1993, *ApJ*, 411, 778
 Balick, B., Wilson, J., & Hajian, A. R. 2001, *AJ*, 121, 354
 Becker, T. 2002, Ph.D. thesis, Univ. Potsdam
 Corradi, R. L. M., Sánchez-Blázquez, P., Mellema, G., Giammanco, C., & Schwarz, H. E. 2004, *A&A*, 417, 637
 Corradi, R. L. M., Schönberner, D., Steffen, M., & Perinotto, M. 2003, *MNRAS*, 340, 417
 Fluks, M. A., Plez, B., The, P. S., de Winter, D., Westerlund, B. E., & Steenman, H. C. 1994, *A&AS*, 105, 311
 Marten, H. 1993, *A&A*, 277, L9
 Méndez, R. H., Kudritzki, R. P., & Herrero, A. 1992, *A&A*, 260, 329
 Middlemass, D., Clegg, R. E. S., & Walsh, J. R. 1989, *MNRAS*, 239, 1
 Middlemass, D., Clegg, R. E. S., Walsh, J. R., & Harrington, J. P. 1991, *MNRAS*, 251, 284
 Perinotto, M., Schönberner, D., Steffen, M., & Calonaci, C. 2004, *A&A*, 414, 993
 Roth, M. M., Schönberner, D., Steffen, M., & Becker, T. 2004, *Astron. Nachr. Suppl.*, 325, 46
 Roth, M. M., et al. 2005, *PASP*, 117, 620
 Schönberner, D., Jacob, R., Steffen, M., Perinotto, M., Corradi, R. L. M., & Acker, A. 2005, *A&A*, 431, 963
 Schönberner, D., & Steffen, M. 2002, *Rev. Mex. AA Ser. Conf.*, 12, 144
 Torres-Peimbert, S., Peimbert, M., & Peña, M. 1990, *A&A*, 233, 540
 Vink, J. S., de Koter, A., & Lamers, H. J. G. L. M. 2001, *A&A*, 369, 574